Paramagnetic NMR Relaxation Enhancement: Spin Dynamics Simulations of the Effect of Zero-Field Splitting Interactions for $S = {}^5/_2$

Jeremy C. Miller and Robert R. Sharp*

Department of Chemistry, The University of Michigan, Ann Arbor, Michigan 48109

Received: February 2, 2000; In Final Form: March 15, 2000

Spin dynamic simulation techniques were used to study the influence of static-zero field splitting (zfs) interactions on the NMR paramagnetic relaxation enhancement (PRE) produced by the spin-$^5/_2$ complex Mn(II)−TSPP (TSPP = tetrakis(sulfonatophenyl)porphyrinate). The NMR-PRE produced by this complex, recently reported by Bryant et al. (*Inorg. Chem.* **1999**, *38*, 1002), has a magnitude and magnetic field dependence that differ markedly from the predictions of the classical Zeeman-limit theory of Solomon, Bloembergen, and Morgan. We show that this failure results from the influence of the static zfs interaction. Inclusion of a zfs coupling of magnitude $D = 0.3$ cm^{-1} in the electron spin Hamiltonian, in conjunction with a realistic description of the effects of Brownian reorientation on the electron spin motion, produced an accurate fit of the experimental T_1 magnetic field dispersion profile. It is shown that the observed dispersion in the NMR-PRE field dispersion profile results from a change in the axis of spatial quantization from a molecule-fixed to a laboratory-fixed axis that occurs as, with increasing Zeeman field strength, the zero-order electron spin Hamiltonian changes from the zfs Hamiltonian to the electronic Zeeman Hamiltonian. The results demonstrate the profound importance of the static zfs interaction in analyses of the NMR paramagnetic relaxation enhancement for $S \geq 1$ ions, even in systems where the static zfs is very small ($|D| < 0.1$ cm^{-1}). They also illustrate the utility of NMR relaxation data for measuring static zfs couplings.

Introduction

Complexes containing $S \geq 1$ paramagnetic metal ions are subject to zero-field splitting (zfs) interactions that can have a very large, frequently controlling, influence on the NMR relaxation properties. High-spin Mn(II), a spin-$^5/_2$ ion with a half-filled d-shell, is generally associated with relatively small zero-field splittings, the order of a few tenths of a wavenumber or less. The magnetic field-dependent NMR relaxation enhancements produced by Mn(II) have been the subject of many previous experimental studies of chemical, biochemical, and medical interest.[1−3] Nearly all previous theoretical analyses in these studies have used Zeeman-limit (Solomon−Bloembergen−Morgan, SBM) theory,[4−6] which neglects the effects of static zfs interactions.

Bryant et al.[7] have recently reported the magnetic field dispersion profile (fdp) of the T_1 relaxation rates produced in the H_2O proton resonance by the $S = {}^5/_2$ complex ion, Mn(II)−TSPP•$(H_2O)_2$ (TSPP = tetrakis(4-sulfonatophenyl)porphyrinate). The qualitative form of the fdp is much broader than the characteristic dispersions of Zeeman-limit (SBM) theory. The authors were unable to fit the fdp using Zeeman-limit theory, except with physically unrealistic values (as they emphasize) for the theoretical parameters. In a discussion of the possible causes of the failure of theory, they suggested that the static zfs interaction might be responsible.

We show here that this is indeed the case: the NMR paramagnetic relaxation enhancement (NMR-PRE) is strongly influenced by the static zfs interaction of Mn(II). An analysis of the experimental data using theory that accounts for both Zeeman and zfs terms in the electron spin Hamiltonian and that incorporates a realistic description of the effects of Brownian reorientation on the electron spin motion simulates the form of the fdp in a straightforward and physically realistic way. It is shown that the physical origin of the T_1 dispersion of Mn(II)−TSPP differs fundamentally from the characteristic dispersions of Zeeman-limit theory. Rather than resulting, as in the Zeeman-limit case, from field dependence in the dipolar spectral density functions (sdf), the dispersion of Mn(II)−TSPP results from the change in the axis of spatial quantization that occurs as, with increasing Zeeman field strength, the zero-order electron spin Hamiltonian changes from the static zfs hamiltonian to the electronic Zeeman Hamiltonian. As the zero-order Hamiltonian changes, the axis of spatial quantization also changes from a molecule-fixed to a laboratory-fixed coordinate frame. Characteristic differences in the two types of T_1 dispersion (referred to below as sdf-type and quantization-type dispersions) are discussed.

The NMR relaxation data provide a direct and sensitive measure of the zfs D-parameter in this system. The high sensitivity of NMR relaxation data to static zfs interactions suggests that zfs effects may likewise be important for understanding the NMR−PRE in other Mn(II)-containing systems, a conclusion reached also by Strandberg and Westlund,[8] in an analysis of Mn(II)−concanavalin A. Many previous analyses that have been based solely on Zeeman-limit (SBM) theory, (as has been the case in nearly all earlier studies of Mn(II)), probably need to be reconsidered.

In the following discussion, we first describe the SD simulation algorithms used in the calculations. It is then shown how incorporation of the static zfs interaction accounts in a straightforward way for the observed NMR relaxation properties.

* Corresponding author. E-mail: rrsharp@umich.edu. FAX: 734-647-4865.

10.1021/jp000418j CCC: $19.00
Published on Web 04/29/2000

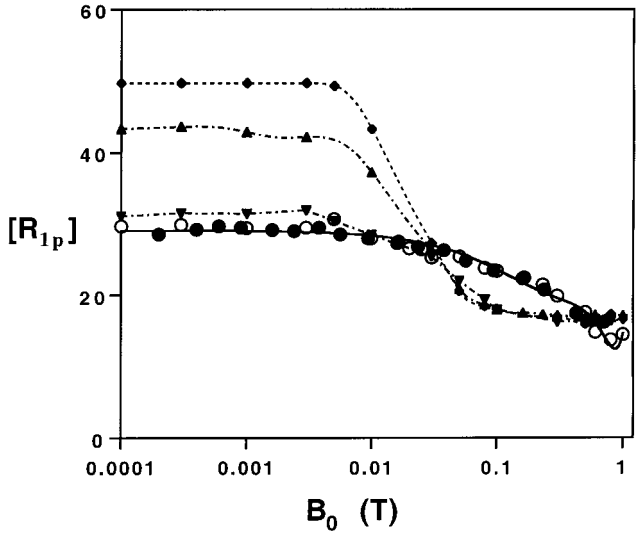

Figure 1. Simulated and experimental NMR-PRE field dispersion profiles for Mn(II)−TSPP. Experimental data (solid circles) are from Bryant et al.[7] SD simulations (dashed curves) were performed using the program RotJmpDyn.f as described in the text. $[R_{1p}]$ is paramagnetic relaxivity, or relaxation rate normalized to a 1 mM concentration. $[R_{1p}]$ is the sum of intra- and intermolecular relaxation contributions, the latter 3−5% of the former. Simulations are shown for the Zeeman-limit (◆, $D = 0$) and for increasing values of $|D| = 0.016$ (▲), 0.05 (▼), and 0.30 cm^{-1} (○). Other parameters are $\tau_S' = 700$ ps, $\tau_R^{(2)} = 500$ ps, $r_{IS} = 0.290$ nm, and $\theta_{\hat{z}} = 0.28$ rad.

Finally the physical mechanism of the NMR-PRE produced by $S = {}^5/_2$ is discussed in some detail and compared with relaxation in the more familiar Zeeman-limit regime. The mechanism of the NMR-PRE depends strongly on the electron spin value, $S = 1$, ${}^3/_2$, 2, and ${}^5/_2$ all exhibiting rather different characteristic relaxation behavior. The mechanistic discussion below focuses on $S = {}^5/_2$.

Data Analysis

The NMR paramagnetic relaxation enhancement (NMR-PRE) is the $T_{1(2)}$ relaxation rate (usually, but not always, of solvent protons) minus the diamagnetic background of the solvent. The axial water ligands of Mn(II)−TSPP are labile, so that the measured R_{1p} is an average quantity reflecting water proton relaxation in the bound (i.e., metal-coordinated) and free (uncoordinated) sites. The measured R_{1p}, which is plotted in Figures 1 and 2 below, can be converted to the intramolecular relaxation rate, R_{1m} ($\equiv T_{1m}^{-1}$), of bound water protons using the Luz−Meiboom equation,[9] $R_{1p} = f_b/(T_{1m} + \tau_{ex}) + R_{1p,os}$. In this expression, f_b is the (bound/free) mole fraction of water protons and τ_{ex} is the mean residence time of a solvent proton in the coordination sphere of the metal ion. For Mn(II), the chemical exchange reactions that transfer water between sites in the coordination sphere are rapid enough that $\tau_{ex} \ll T_{1m}$ (for example, $\tau_{ex} = 4 \times 10^{-8}$ s for $Mn(H_2O)_6^{2+}$),[10−12] and thus it is assumed that $R_{1p} \approx f_b R_{1m} + R_{1p,os}$. $R_{1p,os}$ is an outer-sphere paramagnetic relaxation rate that is usually a few percent of the inner-sphere contribution. In this study, both the inner- and outer-sphere terms, $f_b R_{1m}$ and $R_{1p,os}$, were computed separately by spin dynamics simulation. The outer-sphere term was calculated using a combination of molecular dynamics (MD) and SD simulation techniques in a manner similar to that reported previously.[13,14]

Zfs- and Zeeman-Limit Expressions for R_{1m}. The experimental data for Mn(II)−TSPP span a region of magnetic field strengths varying from the zfs-limit ($H_{zfs} \gg H_{Zeem}$) at the low

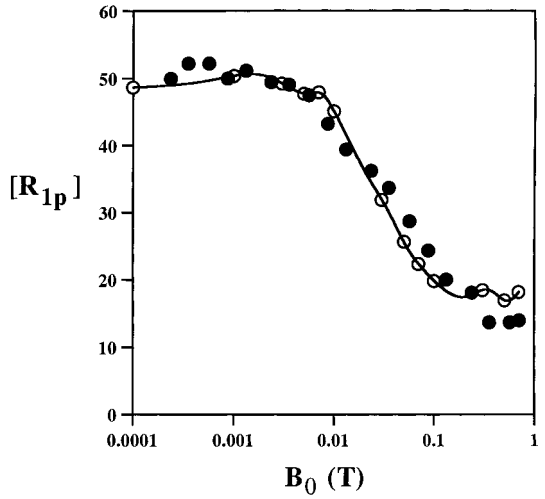

Figure 2. Simulated (○) and experimental (●) NMR-PRE field dispersion profiles[7] for Mn(II)−TSPP−Br_6. The simulation shown is for $D = 0.010$ cm^{-1}. Other parameters are $\tau_S' = 350$ ps, $\tau_R^{(2)} = 600$ ps, $r_{IS} = 0.278$ nm, and $\theta_{\hat{z}} = 0.28$ rad.

end to a regime at the upper end where the Zeeman and zfs interactions are comparable. Zeeman-limit theory[4−6] provides a reference situation against which the importance of zfs interactions can be assessed. The Zeeman-limit dipolar R_{1m} is

$$R_{1m} = R_{1z} + 2R_{1\perp} \tag{1a}$$

$$R_{1z} = (2/15)C[3j(\omega_I)] \tag{1b}$$

$$R_{1\perp} = (1/15)C[6j(\omega_I + \omega_S) + j(\omega_I - \omega_S)] \tag{1c}$$

$$C = (\gamma_I g_e \beta_e)^2 \left(\frac{\mu_o}{4\pi}\right)^2 r_{IS}^{-6} \tag{1d}$$

The quantities γ_I, g_e, β_e, μ_o, and r_{IS} are the nuclear gyromagnetic ratio, the electron g-value, the Bohr magneton, the magnetic permeability of free space, and the I−S interspin distance. For purposes of the ensuing mechanistic discussion, we have written the longitudinal and transverse parts of R_{1m} separately. The quantities R_{1z} and $R_{1\perp}$ arise from local dipolar fields associated with, respectively, the longitudinal and transverse components of the electron spin. They are evaluated from Fourier transforms of the time correlation functions, $\langle S_z(0) \cdot S_z(t) \rangle$ and $\langle S_+(0) \cdot S_-(0)(t) \rangle$ (see below).

The opposite reference situation is the zfs-limit ($B_0 = 0$). For $S = {}^5/_2$ with slow Brownian reorientation,[15] the zfs-limit expressions corresponding to eqs 1 are (taking $\omega_I \ll \omega_D$ and $E = 0$)

$$R_{1m} = R_{1\hat{z}} + 2R_{1\hat{\perp}} \tag{2a}$$

$$R_{1\hat{z}} = (2/9)C[(1 + P_2(\cos\theta_{\hat{z}}))(35/2)j(\omega_I)] \tag{2b}$$

$$R_{1\hat{\perp}} = (2/9)C[2 - P_2(\cos\theta_{\hat{z}})]((9/4)j(\omega_I) + 4j(2\omega_D) + (5/2)j(4\omega_D))]. \tag{2c}$$

As for the Zeeman-limit case, the longitudinal and transverse components of R_{1m}, defined in eqs 2 in the molecular frame, are additive and have been written separately. Unlike the Zeeman-limit expression, the zfs-limit result depends on the orientation of the I−S vector with respect to the molecule-fixed zfs principal axis system (the zfs-PAS, $\hat{x}$, $\hat{y}$, $\hat{z}$). $\theta_{\hat{z}}$ is the angle

of the I−S vector with respect to $\hat{z}$, and $P_2(x)$ is the second-order Legendre polynomial. With a cylindrical zfs tensor, the factor $[2\text{-}P_2(\cos\theta_{\hat{z}})]$ accounts for both transverse contributions $(\hat{x}, \hat{y})$ to R_{1p}.

The $j(\omega)$ in eqs 1 and 2 are spectral density functions (sdf's) describing the dipolar power density. In the limiting theories (eqs 1 and 3), the sdf's are assumed to have a Lorentzian form $j(\omega) = \tau_d(1 + \omega^2\tau_d^2)^{-1}$, corresponding to an exponential decay of the dipole−dipole TCF's. τ_d is a correlation time for the I−S dipole−dipole interaction, given by

$$\tau_d^{-1} = (\tau_R^{(2)})^{-1} + \tau_S^{-1} + \tau_{ex}^{-1} \tag{3}$$

τ_d contains contributions from the stochastic processes that randomize the I−S dipole−dipole interaction: these include (1) Brownian reorientation, with a correlation time $\tau_R^{(2)}$; (2) electron spin relaxation (τ_S); and, when the ligand is labile, (3) chemical exchange reactions. τ_{ex} is the mean residence time of a water proton in the bound site prior to a chemical exchange event.

Spin Dynamics Simulation Methods. To calculate the NMR-PRE in the intermediate regime where the Zeeman and zfs energies are comparable and where the molecule undergoes rapid Brownian reorientation, SD simulation methods were used. The algorithms are implemented in the computer program RotJmpDyn.f, which is a refined and extended version of the program described in ref 16. SD simulations of the NMR-PRE are analogous in spirit to molecular dynamics (MD) simulations, except that the matrix elements of the electron spin operators are propagated in the time domain using the QM equation of the spin motion rather than, as in MD, propagating molecular coordinates in the time domain using the Newtonian equations of motion. In this way, the fundamental quantities of spin relaxation theory, which are the time correlation functions (TCF's) of the spin operators, $G_r(r) = \overline{\langle S_r(0)\cdot S_r(r)\rangle}$, ($r = 0, \pm1$, or $\hat{x}, \hat{y}, \hat{z}$), are calculated across a trajectory of finite time steps. The resulting trajectories of the spin matrix elements are averaged over an ensemble of several thousand trajectories. The starting molecular reorientation for each trajectory is defined by the polar angles of one of the 92 vertices and face centers of the truncated icosahedron (buckyball); this provides effective isotropic spatial averaging of the molecular axes with respect to the Zeeman axis. At the end of each time step in a given trajectory, the molecular axes of the solute are rotated by an algorithm that simulates Brownian reorientation: the molecule is rotated about a randomly oriented axis through a rotational angle that is computed as a Gaussian deviate of zero mean, the standard deviation of which is selected to simulate the desired reorientational correlation time. Following each reorientation event, the new spin Hamiltonian and spin propagator are computed and the process of spin propagation is repeated. The spherical harmonics of the interspin vector needed to compute the nuclear−electron dipole−dipole coupling tensor are also computed at each orientation. The time correlation functions of the dipole−dipole coupling energy are then computed as statistical mechanical averages composed of 92*n* trajectories, each comprised of 50 to several thousand time points, with an interval selected as required to describe temporal variations in the TCF. The stochastic noise of the simulation is determined by *n*, which is typically set to a value from 4 to 16, giving scatter of about ±5% in the simulated T_{1m}'s.

Electron Spin Relaxation. The electron spin relaxation time in eq 3 is a relatively complex quantity that is in general magnetic field-dependent. It is in general a sum of three terms due to collisional,[6,17] vibrational,[18] and reorientational[19] modulation of the zfs interaction

$$\tau_S^{-1} = \tau_{S,c}^{-1} + \tau_{S,v}^{-1} + \tau_{S,R}^{-1} \tag{4}$$

The most widely used theoretical description of τ_S is that of Bloembergen and Morgan (B−M),[6] which assumes that electron spin relaxation results from stochastic modulation of the zfs tensor due to Brownian collisions of the solute and solvent. Thus B−M theory calculates $\tau_{S,c}$. Taking Δ_t^2 as the trace of the transient part of the mean-square zfs tensor and τ_v as the correlation time for collisional zfs fluctuations, B−M theory gives

$$\tau_{S,c}^{-1} = (\Delta_t^2\tau_v/5)[1/(1 + \omega_S^2\tau_v^2) + 4/(1 + 4\omega_S^2\tau_v^2)] \tag{5}$$

Analogous zfs-limit expressions for $\tau_{S,c}$ for $S = 1$ have also been given.[20,21]

Reorientational modulation of the permanent (i.e., vibrationally and collisionally averaged) zfs tensor provides a second relaxation mechanism ($\tau_{S,R}$), for which the correlation time is $\tau_R^{(2)}$. This relaxation mechanism vanishes when the static zfs interaction is absent, as occurs for many hexaaquo metal cations, but it becomes quite important when a static zfs coupling is present and when molecular reorientation is reasonably rapid (i.e., not too much longer than τ_S). We show below that for Mn(II)−TSPP, $(\tau_{S,R})^{-1}$ is in fact the largest term in eq 4. The SD algorithms account directly for the effects of $\tau_{S,R}$, since the electron spin Hamiltonian and propagator are reevaluated in the new molecular orientation at each time point in the SD trajectory. The effects of Brownian reorientation as a cause of thermal decay of the spin TCF's, including magnetic field dependence, are thus described implicitly by the SD algorithms, and no independent parametrization of $\tau_{S,R}$ is required.

The third contribution, $\tau_{S,v}^{-1}$, arises from vibrational modulation of the zfs tensor (Al'tshuler and Valiev[18]), a process that has stochastic character associated with thermal excitation and deexcitation of vibrational modes involving the metal coordination sphere. The vibrational mechanism is essentially independent of the Zeeman field strength. This contribution has been neglected in most previous studies, although there is little specific experimental or computational justification for this assumption,[22] which seems questionable particularly for complexes in which the metal coordination sphere is well shielded from the solvent. In the low-field region where $2\omega_S\tau_v > 1$, the collisional and vibrational terms in eq 4 can be described by a single quantity, $\tau_S'^{-1} = \tau_{S,c}^{-1} + \tau_{S,v}^{-1}$. Most of the SD simulations assumed a single field-independent parameter τ_S' to describe the composite collisional/vibrational relaxation mechanism.

Results

Figures 1 and 2 show the experimental T_1 fdp's (solid circles) for Mn(II)−TSPP and Mn(II)−TSPP−Br_6, taken from Bryant et al.[7] The various curves in the figures summarize the results of SD simulation studies described below. The next section discusses the physics of the NMR-PRE relaxation mechanism for $S = {}^5/_2$ in the presence of competing Zeeman and zfs interactions.

The calculated Zeeman-limit dipolar fdp for Mn(II)−TSPP is shown by the dashed line in Figure 1. As has been described in considerable detail by Bryant et al.,[7] Zeeman-limit theory is incapable of fitting the experimental data satisfactorily except by using parameter sets that are almost certainly physically unrealistic. The width, the amplitude, and the midfield position

of the observed T_1 dispersion are all difficult to explain using Zeeman-limit theory. Using SD simulation techniques, we have extended the analysis to include a static cylindrical zfs term (a zfs D parameter) in the electron spin Hamiltonian. The NMR-PRE depends on six theoretical parameters, of which four are known (or tightly constrained) by other experiments. These include two molecular structure parameters, r_{IS} and $\theta_{\hat{x}}$; the reorientational correlation time τ_R; and three spin paramters, D, τ_S', and τ_v. (The zfs rhombic parameter E vanishes in the four-fold site symmetry of the Mn(II) ion). For Mn(II), the g-value is isotropic and approximately equal to the free-electron g-value, $g_e = 2.00$.

The molecular structure parameters, r_{IS} and $\theta_{\hat{z}}$, describe the length and polar angle of the interspin I−S vector with respect to the molecular coordinate frame; the values used were $r_{IS} = 0.290$ nm and $\theta_{\hat{z}} = 16°$. Calculations of R_{1m} scale as r_{IS}^{-6}. The value of r_{IS} is not known precisely, but the assumed value, which is 0.12 Å longer than for $Mn(II)(H_2O)_6^{2+}$, is reasonable and gave an excellent fit to the experimental data. The polar angle, $\theta_{\hat{z}} = 16°$, is representative of O−M−H angles for metal-coordinated water derived from neutron diffraction experiments on aqueous solutions of divalent metal ions.[23] Small variations in this angle the order of ±5° have little effect on the simulations.

The SD simulations assumed a dipolar correlation time of the form of eq 3 but neglected τ_{ex}^{-1}, which is expected to be much smaller than the other quantities. For H_2O ligands to Mn(II), τ_{ex} is in the range[10−12] 10^{-8}−10^{-7} s, which is 2−3 orders of magnitude longer than $\tau_R^{(2)}$. $\tau_R^{(2)}$ has been measured by ^{13}C T_1 relaxation for the diamagnetic analogue, Zn(II)−TSPP/H_2O. The measured value,[7] 275 ps at 298 K, was adjusted to $T = 3$ °C using the Debye equation[24] ($\tau_R^{(2)} \propto \eta/T$) and the tabulated viscosity (η) of water, giving $\tau_R^{(2)} = 500$ ps (3 °C). τ_S^{-1} was calculated as described in the previous section. The reorientational part, $(\tau_{S,R})^{-1}$, of τ_S^{-1} (including the magnetic field dependence) is calculated directly by the SD algorithms without independent parametrization. The collisional and vibrational parts of τ_S^{-1} were described using an adjustable, field-independent parameter τ_S', an assumption that appeared warranted (see below) within the range of experimental data ($B_0 <$ 0.7 T).

Taking the parameters (r_{IS}, $\theta_{\hat{z}}$, τ_R) as fixed, SD simulations were performed varying D and τ_S', the latter initially assumed to be field-independent. A family of fdp's, simulated for Mn(II)−TSPP with increasing D, is shown as the dashed lines in Figure 1. In the limit $D \rightarrow 0$, the results of the SD simulations approached the Zeeman-limit profile computed using eq 1. The introduction of quite small nonzero D parameters the order of a few hundredths of a wavenumber caused a dramatic suppression of the low-field T_1 dispersion. This effect was nearly maximal at $D = 0.05$ cm^{-1}. Values of $|D|$ larger than about 0.1 cm^{-1} markedly broadened the dispersion and displaced the midfield value to higher B_0. A quantitative fit to the data was obtained using $|D| = 0.32 \pm 0.07$ cm^{-1}, $\tau_S' = 700$ ps. The uncertainty in $|D|$ was estimated by bracketing the experimental data with simulated fdp's.

The simulated fdp's in Figures 1 and 2 contain both the inter- and intramolecular contributions to R_{1p}. The intermolecular part of R_{1p} was calculated using SD simulation. This component was 3−5% of the intramolecular R_{1p} and thus, while not quite insignificant, was of minor importance. The calculations were carried out as described previously,[13] using molecular dynamics simulation (Cerius2: Biosym/MSI, Inc.) to compute the I−S "distance of closest approach". In a recent study,[14] we compared a measured intermolecular R_{1p} with the results of SD/MD simulations performed in a similar manner, and the results were in agreement within 5%.

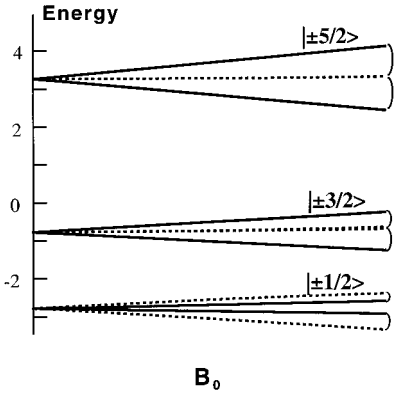

Figure 3. Energy level diagram for $S = 5/2$ in the presence of a uniaxial zfs interaction plus a smaller Zeeman interaction in a powdered sample. The vertical scale is energy in units of $\hbar\omega_D = hcD$ (D is the zfs parameter in wavenumbers). The diagram assumes a positive D; a negative D inverts the levels.

Most of the SD simulations were performed assuming a field-independent parameter τ_S'. As shown in Figure 1, this assumption gave excellent agreement with the experimental data. To test for a possible field dependence in τ_S', simulations were also performed using the B−M expression for $\tau_S' = \tau_{S,c}$, with τ_v in the range 1−6 ps. For $\tau_v \leq 4$ ps, the simulated profiles were essentially indistinguishable from those which assumed a field-independent τ_S'. A value of $\tau_v = 6$ ps produced a slight upturn at the high-field end of the simulated profile that was not reflected in the experimental data, and we thus concluded that τ_S' is to a good approximation field-independent across the experimental range.

Figure 2 shows simulated and experimental[7] T_1 fdp's for Mn(II)−TSPP−Br_6. The amplitude and width of the low-field dispersion for Mn(II)−TSPP−Br_6, relative to that for Mn(II)−TSPP, suggest a considerably smaller static D-parameter in the former, and this was, in fact, confirmed in simulations. In the SD simulations, τ_R was corrected using Debye's equation,[24] $\tau_R = V_m\eta/kT$, with molecular volumes evaluated by the modeling program Cerius2 (Biosym/MSI Inc.). This procedure gave $\tau_R^{(2)} = 590$ ps (3 °C). A fairly good fit to the data was obtained using $|D| = 0.010 \pm 0.003$ cm^{-1}, $\tau_S' = 350$ ps (see Figure 2). This fit required a somewhat shorter I−S distance, $r_{IS} = 0.278$ nm, than was used for Mn(II)−TSPP.

Discussion

To describe the physical relaxation mechanism, we refer to the $S = 5/2$ spin level diagram in Figure 3. In the zfs-limit, a nonzero D term splits the $S = 5/2$ levels in a slowly reorienting molecule into three Kramers doublets, $m_S = \pm 1/2, \pm 3/2, \pm 5/2$, with energies (in units of $\hbar$) of $-8/3\omega_D$, $-2/3\omega_D$, and $+10/3\omega_D$ rad s^{-1}. The addition of a Zeeman interaction splits the Kramers doublets and broadens the levels into a band structure owing to the fact that the energy depends on the orientation of B_0 with respect to the molecular $\hat{z}$-axis.

Dipolar Power Plots. The spin level structure of Figure 3 underlies, and is reflected in, the NMR-PRE field dispersion profile. The structure of the relaxation mechanism is most readily visualized through dipolar power density plots, which illustrate graphically many aspects of the relaxation mechanism. Dipolar power plots are based on the slow-reorientation theory of ref 15, of which eqs 1 and 2 are limiting forms for $S = 5/2$.

The NMR-PRE in the slow-reorientation limit is a sum of relaxation contributions of the form

$$R_{1m,r} = C_r \sum_{i,j} |\langle i|S_r|j\rangle|^2 j(\omega_{ij}) \tag{6}$$

The index r labels spatial coordinates, which in the Zeeman-basis formulation are usually taken to be circular coordinates ($r = 0, \pm 1$) or in the zfs-basis, molecular-frame Cartesian coordinates ($r = \hat{x}, \hat{y}, \hat{z}$). Dipolar power density plots are plots of the functions $J_{ij}^{(r)}(\omega) \equiv |\langle i|S_r|j\rangle|^2 j(\omega_{ij} - \omega)$ against ω. These functions provide an approximate measure[25] of the dipolar power density associated with a given electronic transition (i, j) and spatial polarization of spin motion (r). The power density at $\omega = \omega_I$ is proportional to the T_1 NMR relaxation efficiency.

As an illustration, the classical Zeeman-limit T_1 fdp consists of two dispersions with amplitudes in the ratio 3:7, arising from R_{1z} and $R_{1\perp}$ in eqs 1, respectively. The Zeeman-limit NMR T_1 fdp is shown as a dashed curve in Figure 1. The corresponding Zeeman-limit dipolar power density plot is shown in Figure 4. The two power bands shown as solid and dashed lines describe, respectively, the longitudinal and transverse power density functions, summed over spin eigenstates:

$$G_z(\omega) \equiv \sum_i J_{ii}^{(z)}(\omega) \tag{7a}$$

$$G\perp(\omega) \equiv \sum_{i,j} (J_{ij}^{(x)}(\omega) + J_{ij}^{(y)}(\omega)) \tag{7b}$$

The longitudinal band, $G_z(\omega)$, is a Lorenzian function centered at $\omega = \omega_I \approx 0$, independent of ω_S, since $\langle S_z(0) \cdot S_z(t)\rangle$ is constant with respect to precession. This behavior is implied by the semiclassical precessional picture of the Zeeman-limit in which $\langle S_z\rangle$ is a constant of the motion. The transverse power density function, $G_\perp(\omega)$, is a Lorentzian of width $2\tau_d^{-1}$ centered at ω_S; i.e., it is offset from $\omega = 0$ owing to the precessional motion of $\langle S_\perp(0) \cdot S_\perp(t)\rangle$. The low-field T_1 dispersion of the Zeeman-limit field dispersion profile results from the magnetic field dependence of the transverse power band ($G_\perp(\omega)$), which, unlike the longitudinal band, is centered at ω_S and hence depends on B_0. The NMR relaxation efficiency is proportional to the dipolar power at $\omega = \omega_I \approx 0$, which, for the transverse band, disperses away with increasing B_0 as the center of the power band is displaced from ω_I. We refer to a dispersion of this kind resulting from magnetic field dependence in spectral density functions (sdf) as an sdf-type dispersion.[26] Sdf dispersions are characteristic of the Zeeman-limit.

The zfs-limit situation can be described by an analogous power plot, except that there are three 1Q frequencies ($\omega = 0$, $2\omega_D$, and $4\omega_D$) that are fixed by the static zfs interaction. The T_1 dispersion of the Zeeman-limit fdp is absent in the zfs-limit situation, where the 1Q level splittings are approximately magnetic field-independent. The potent effect of a very small zfs in suppressing the low-field sdf-type dispersion, as occurs in the simulations of Figure 1, reflects this phenomenon. As shown in Figure 5, a nonzero zfs interaction increases the 1Q transition frequencies at $2\omega_D$ and $4\omega_D$, thereby suppressing the influence of the dipolar power bands centered at $2\omega_D$ and $4\omega_D$. In addition to the dramatic decrease in amplitude, the sdf-type dispersion broadens somewhat with increasing D and is displaced to a slightly higher midfield value owing to changes in the energy band structure shown in Figure 3.

SDF- and Quantization-type Dispersions. In the simulations of Figure 1, the suppression of the low-field dispersion is essentially complete at $D = 0.05$ cm^{-1}. At higher D values, further changes in the form of the fdp occur: the midfield value of the dispersion shifts to a substantially higher field strength, while the form of the fdp broadens considerably and becomes more complex in shape. This second set of phenomena (occurring in the range $D = 0.1 - 0.6$ cm^{-1} in Figure 1) have the *superficial* appearance of modified sdf-type dispersion, but their physical origin is actually quite different. In this regime, only the low-frequency sdf's $j(\omega_I)$ contribute significantly, and these do not disperse; the terms depending on $j(2\omega_D)$ and $j(4\omega_D)$ are negligible, and thus there is no significant sdf-type dispersion (Figure 5). The changes in the simulated fdp's result rather from the change in spatial quantization that occurs on passing from

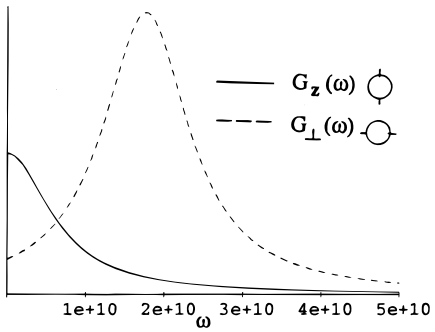

Figure 4. Dipolar power density plot illustrating the Zeeman-limit situation. The solid and dashed curves are plots of the summed longitudinal and transverse power functions, $G_z(\omega)$ and $G_\perp(\omega)$, respectively. The small spherical figures indicate that the associated R_{1p} contribution does not depend on the orientation of the interspin I−S vector with respect to the molecular coordinate frame.

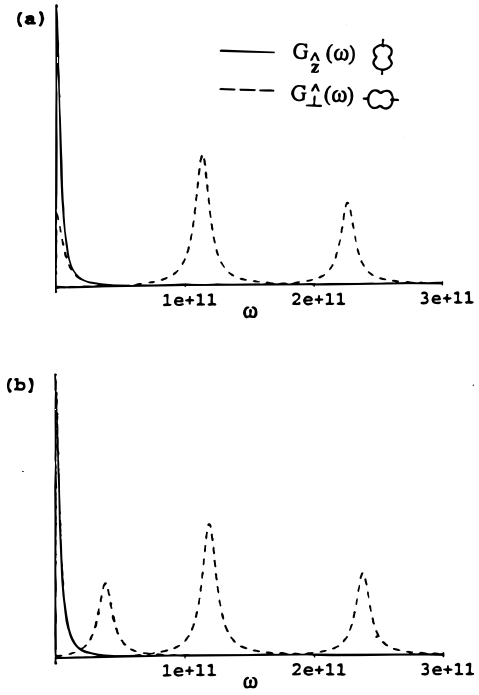

Figure 5. Dipolar power density plots for $S = {}^5/_2$, computed using theoretical parameters, $|D| = 0.3$ cm^{-1} and $\tau_S' = 700$ ps ($\tau_d = 290$ ps), corresponding to Mn(II)−TSPP (Figure 1, open circles). Plots are shown for (a) the zfs-limit ($B_0 = 0$) and (b) a Zeeman field strength of 0.1 T. The solid curve is a plot of the summed longitudinal power function, $G_{\hat{z}}(\omega)$. The dashed curves, summed together, give the transverse power function, $G_{\hat{\perp}}(\omega)$. The three component bands of $G_{\hat{\perp}}(\omega)$ arise from the three 1Q transitions, which in order of increasing ω are $(+{}^1/_2 \leftrightarrow -{}^1/_2)$, $(\pm{}^1/_2 \leftrightarrow \pm{}^3/_2)$, and $(\pm{}^3/_2 \leftrightarrow \pm{}^5/_2)$. The small bilobed figures indicate a $(1 + P_2(\cos\theta_{\hat{z}(\perp)}))$ dependence on the orientation of the I−S vector with respect to the molecule-fixed coordinate frame.

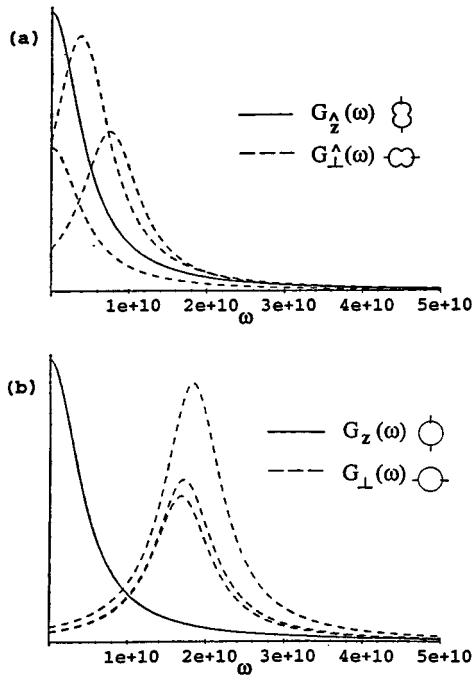

Figure 6. Dipolar power density plots for $S = {}^5/_2$, computed using theoretical parameters, $|D| = 0.010$ cm^{-1} and $\tau_S' = 350$ ps ($\tau_d = 220$ ps), corresponding to Mn(II)−TSPP−Br_6 (Figure 2). Plots are shown for (a) the zfs-limit ($B_0 = 0$) and (b) a Zeeman field strength of 0.1 T. The solid and dashed curves correspond to the molecular-frame longitudinal and transverse dipolar power functions as described in the legend of Figure 5.

the zfs- to the Zeeman-limit regime. In the zfs-limit, the electron spin precessional motion is quantized with respect to the molecule-fixed zfs-PAS rather than along the Zeeman field. When, in a rising magnetic field, the Zeeman energy exceeds the zfs energy, the spatial quantization changes from molecular-frame quantization to laboratory-frame quantization. The low-field dispersion observed for Mn(II)−TSPP is of this second type—it results from the changing spatial quantization of the electron spin motion rather than from magnetic field dependence in the sdf's.

The quantization-type dispersion is clearly much broader than the sdf-type dispersions of Zeeman-limit theory. In addition, the shape of the quantization-type dispersion is not simple but depends rather strongly on the orientation of the I−S vector with respect to the zfs-PAS.[14,27] Qualitatively, axial positions of the nuclear spin are more strongly relaxing in the zfs-limit than are equatorial positions. As a consequence, quantization-type dispersions at axial positions exhibit a decrease of R_1 with increasing Zeeman field strength, as in Figure 1, while the dispersions associated with equatorial nuclear positions produce "inverted" dispersions, where R_{1m} rises with increasing field strength.[27] This dependence on orientation of the I−S vector is a reflection of the geometry of the local mean-square dipolar field produced by the electron spin in M−F quantization, and it is described in the slow-reorientation situation by the factors $(1 + P_2((\cos \theta_{\hat{z}(\perp)})$ in eqs 2. Other examples of the dependence of quantization-type dispersions on the orientation of the I−S vector for various spin values are described in ref 27.

The zfs D parameter is considerably smaller for the brominated complex Mn(II)−TSPP−Br_6 (Figure 2) than for the unbrominated complex (Figure 1). The dipolar power plot (Figure 6) shows substantial zero frequency power associated with the transverse spin components in the zfs-limit (Figure 6a), which disperses away with increasing B_0 (Figure 6b). For this complex, the dispersion is better described as sdf-type than quantization-type, although the character is substantially mixed.

Dependence on Orientation of the I−S Interspin Vector. In the zfs-limit, the NMR relaxation efficiency depends on the orientation of the I−S interspin vector with respect to the molecular coordinate frame as described by the factors $(1 + P_2(\cos \theta_r))$ in eq 2. This aspect of theory has recently been confirmed by a measurement of the zfs-limit axial/equatorial R_{1p} ratio in the $S = 1$ complex [Ni(II)$acac_2(H_2O)_2$]. This kind of spatial anisotropy is illustrated by the small "dumbbell"-like figures in the dipolar power density plots (Figures 5 and 6). In Figure 5, the associated geometric factor is oriented along $\hat{z}$ for the $G_{\hat{z}}(\omega)$ band; hence, that contribution to R_{1p} is larger at axial nuclear orientations ($\hat{z}$) than at equatorial orientations ($\hat{\perp}$), the axial/equatorial ratio being 4:1. For the $G_{\hat{\perp}}(\omega)$ band, the angular dependence is inverted: NMR relaxation associated with that power band is more efficient at equatorial nuclear positions than equatorial, the axial/equatorial ratio being 1:4. Since the zero-frequency longitudinal power is much greater than the zero-frequency transverse power, the total relaxation efficiency exhibits approximately a 4:1 axial/equatorial ratio. In the Zeeman-limit, this dependence on the orientation of the I−S vector disappears, since the orientation of the local dipolar field of S is then uncorrelated with the orientation of the molecule. Hence the geometric factor for the Zeeman-limit diagram (Figure 4) and near Zeeman-limit case of Figure 6b is depicted as a sphere.

Conclusions

(1) For paramagnetic ions with spins $S \geq 1$, the influence of static zfs couplings must be included in the theoretical description of the NMR-PRE when the Zeeman energy is smaller than or comparable to the largest zfs level splittings. (Expressed in terms of the zfs frequency ω_D, the largest zfs splittings for spins $S = 1$, ${}^3/_2$, 2, and ${}^5/_2$ are ω_D, $2\omega_D$, $4\omega_D$, and $6\omega_D$, respectively). The computer program RotJmpDyn.f provides a flexible and user-friendly (we hope) platform for these calculations and is available on request.

(2) Static zfs couplings can produce dispersions that differ markedly in functional form from the characteristic dispersions of Zeeman-limit theory. These dispersions result physically from a magnetic field-induced change in the axes of spatial quantization of the electron spin motion, rather than, as in the Zeeman-limit, from magnetic field dependence of spectral density functions.

(3) Variable field NMR relaxometry offers a sensitive way of measuring quite small zfs parameters. As we have pointed out in earlier work,[28] the NMR-PRE for spins $S \geq 1$ exhibits a truly remarkable dependence on the presence of very small zfs splittings, in some cases providing a unique window for their measurement.

(4) Mn(II), which is probably the most widely studied ion with respect to paramagnetic NMR relaxation enhancement, typically exhibits quite small static zfs couplings, the order of at most a few tenths of a wavenumber. The neglect of even these small static zfs effects in analyses of NMR T_1 field dispersion profile data is likely to introduce serious error into the analysis (see also Strandberg and Westlund[8]). Most previous NMR relaxometry studies of $S \geq 1$ systems have been analyzed using Zeeman-limit (SBM) theory; where the static site symmetry of the metal ion is noncubic, these need to be reassessed with respect to the likely influence of the static zfs interaction.

Acknowledgment. This research was supported by the U.S. National Science Foundation in the form of a research grant, CHE-9423351.

References and Notes

(1) Dwek, R. A. *NMR in Biology*; Academic: London, 1977.
(2) Banci, L.; Bertini, I.; Luchinat, C. *Nuclear and Electron Relaxation*; VCH Publishers: Weinheim, Germany, 1991.
(3) Bertini, I.; Luchinat, *C. Coord. Chem. Rev.* **1996**, 150.
(4) Solomon, I. *Phys. Rev.* **1955**, *99*, 555.
(5) Bloembergen, N. *J. Chem. Phys.* **1957**, *34*, 842.
(6) Bloembergen, N.; Morgan, L. O. *J. Chem. Phys.* **1961**, *34*, 842.
(7) Bryant, L. H.; Hodges, M. W.; Bryant, R. G. *Inorg. Chem.* **1999**, *38*, 1002.
(8) Strandberg, E.; Westlund, P.-O. *J. Magn. Reson.* **1999**, *137*, 333.
(9) Luz, Z.; Meiboom, S. *J Chem. Phys.* **1965**, *40*, 2686.
(10) Luz, Z.; Shulman, R. G. *J. Chem. Phys*. **1965**, *43*, 3750.
(11) Bernheim, R. A.; Brown, T. H.; Gutowsky, H. S.; Woessner, D. E. *J. Chem. Phys.* **1959**, *30*, 950.
(12) Koenig, S. H.; Brown, R. D.; Studebaker, H. D. *J. Cold Spring Harbor Symp. Quant. Biol*. **1974**, *36*, 551.
(13) Abernathy, S. M.; R. R. Sharp, R. R. *J. Phys. Chem.* **1997**, *101*, 3692.
(14) Miller, J. C.; Abernathy, S. M.; Sharp, R. R. *J. Phys. Chem.*, in press.
(15) Sharp, R. R.; Abernathy, S. M.; Lohr, L. L. *J. Chem. Phys.* **1997**, *107*, 7620.
(16) Abernathy, S. M.; Sharp, R. R. *J. Chem. Phys.* **1977**, *106*, 9032.
(17) M. Rubinstein, M.; Baram, A; Luz, Z. *Mol. Phys.* **1971**, *20*, 67.
(18) Al'tshuler, S. A.; Valiev, K. A. *Sov. Phys. JETP* **1959**, *35*, 661.
(19) Carrington, A.; Luckhurst, G. R. *Mol. Phys.* **1964**, *8*, 125.
(20) Westlund, P. O. *J. Chem. Phys* **1998**, *108*, 4945.
(21) Bertini, C.; Kowalewski, J.; Luchinat, C.; Nilsson, T.; Parigi, G. *J. Chem. Phys.* **1999**, *111*, 5795.
(22) The most extensive examination of the point was undertaken by Odelius et al. with respect to the Ni(II) hexaqua cation: Odelius, M.; Ribbing, C.; Kowalewski, J. *J. Chem. Phys.* **1995**, *103*, 1800; *J. Chem. Phys.* **1996**, *104*, 3181.
(23) Powell, D. H. *J. Phys.: Condens. Matter* **1989**, *1*, 8721.
(24) Abragam, A. *The Principles of Nuclear Magnetism*; Oxford University: London; 1961; Chapter 8.
(25) The $J_{ij}^{(r)}(\omega_I)$ do not contain two factors of order unity that appear in eq 2, and thus they are not quantitatively proportional to NMR relaxation efficiency. The factors omitted are geometrical, involving (1) a product of 3-*j* symbols and (2) a factor describing the dependence on the orientation of the interspin I−S vector in the molecular coordinate frame. The $J_{ij}^{(r)}(\omega_I)$, while not strictly proportional to NMR relaxation efficiency, are nevertheless very useful for describing the properties of individual spin transitions with respect to their contributions to the NMR-PRE.
(26) A "high-field" sdf-type dispersion associated with $j(\omega_I)$ in eq 1 occurs at very high (usually unobservable) Zeeman field strengths. This dispersion occurs when ω_I is shifted out from under the zero-frequency dipolar power band.
(27) Sharp, R. R. *J. Chem. Phys.* **1993**, *98*, 2507.
(28) Abernathy, S. M.; Miller, J. C.; Lohr, L. L.; Sharp, R. R. *J. Chem. Phys.* **1998**, *109*, 4035.